Supplementary information for

Revealing the importance of non-radical mechanisms in the degradation of sulfamethazine by Lewis acid-etched Co@MXene-activated peroxyacetic acid

Dezhu Liu[a], Siling Zhang[a], Zhenwei Zou[a], Zheng Fang[ab], Ping Chen[a], Zongshun Yu[a], Xiaoyu Zhang[a], Zhenchao Li[a], Zili Lin[a], Wenying Lv[a*], Guoguang Liu[a*]

[a]*Guangdong Key Laboratory of Environmental Catalysis and Health Risk Control, School of Environmental Science and Engineering, Institute of Environmental Health and Pollution Control, Guangdong University of Technology, Guangzhou 510006, China*

[b]*State Key Laboratory of Biogeology and Environmental Geology, China University of Geosciences, Wuhan, 430078, China*

*** Corresponding Author:** Wenying Lv; Guoguang Liu

E-mail: lvwy612@163.com; liugg615@163.com;

Phone: +86-13533635690, Fax: +86-20-3932254.

Text

Text S1. Materials

Commercial peroxyacetic acid was purchased from Tianjin Damao Chemical Reagent Factory, MAX phase Ti_3AlC_2, cobalt chloride hexahydrate was purchased from Shanghai McLean Biochemistry Science and Technology Co. Chemicals such as 5,5-dimethyl-1-pyrroline-N-oxide, 4-hydroxy-TEMPO, 2,2,6,6-tetramethylpiperidine, tert-butanol, β-carotene, p-benzoquinone, sodium chloride, sodium sulfate, sodium hydroxide, sulfamerazine, sulfanilamide, sulfamethoxazole, sulfafurazole, sodium carbonate, and Nafion™ perfluorinated resin solution were purchased from Aladdin Company. The purity of all the above chemicals was higher than analytical purity and no further purification was required. Hydrochloric acid, sulfuric acid and other reagents were purchased from Guangzhou Reagent Factory. Acetonitrile, methanol and other chromatographic pure grade reagents were purchased from Shanghai Amperexperiment Technology Co. High purity nitrogen, high purity oxygen and high purity argon were procured from Messer.

Text S2. Analytic methods

The catalytic degradation experiments with different variables were carried out using the controlled variable method of experimentally relevant factors. The catalytic degradation experiments were carried out in a 100 ml glass beaker at room temperature with constant stirring at 400 rpm. First, a quantity of catalyst was added to 100 ml of a solution spiked with 10 mg/litre of organic pollutant for 30 minutes to reach adsorption-desorption equilibrium. A quantity of PAA was then added to the solution to initiate the degradation reaction. If necessary, the initial pH of the water was adjusted with 0.1 M HCl or 0.1 M NaOH.

Concentrations of organic pollutants were determined by high performance liquid chromatography (HPLC, Shimadzu LC16), and the separation was performed on a C18 column (Eclipse Plus, 250 mm × 4.6 mm × 5 μm). The mobile phase was methanol: formic acid water = 40 %: 60 %, and the UV detection wavelength was 254 nm. PAA was detected by the method of chemical probe with the specific values as described in Ref[1]. The mobile phase was acetonitrile: ultrapure water = 50 %: 50 %. The sample concentrations obtained were analysed and processed using first order kinetic equation. The equation is given below:

$$\ln(C_0/C_t) = kt \quad \text{(Eq. 1)}$$

Spin-polarized electronic structure calculations were performed using the plane-wave basis set approach as implemented in the Vienna ab initio simulation package (VASP) [2]. The projector augmented wave (PAW) method was used to represent the ion–core electron interactions [3]. The valence electrons were represented with a plane wave basis set with an energy cutoff of 450 eV. Electronic exchange and correlation were described with the Perdew–Burke–Ernzerhof (PBE) functional [4]. DFT-D3 method was used to treat the van der Waals interaction [5]. A 2×2×1 Monkhorst–Pack scheme was used to generate the k-point grid for the modeled surfaces [6]. The convergence criteria for the self-consistent electronic structure and geometry were set to 10^{-5} eV and 0.05 eV/Å, respectively. Zero-point vibrational energy (ZPVE) corrections are calculated by assuming a quantum harmonic oscillator possessing the calculated vibrational frequency. Transition state calculations were performed using the climbing image nudged elastic band (CI-NEB) method with the transition state identified to have an absolute tangent force below 0.05 eV/Å [7]. Adsorption energies were calculated

as:

$$\Delta E_{ads} = E_{tot}-E_{sur}-E_{mol} \quad \text{(Eq. 2)}$$

where E_{tot}, E_{sur}, and E_{mol} indicate the total energy of molecules on surfaces, energy of bare surfaces, and energy of the molecule in vacuum, respectively. Reaction energies, ΔE_{rxn}, and activation barriers, ΔE_{act}, were defined as follows.

$$\Delta E_{rxn}=E_{final}-E_{initial} \quad \text{(Eq. 3)}$$

Table S1. Ti and Co in Co@MXene determined by ablation-ICP/MS and EDS

	ICP-MS	EDS (SEM)
Co	16.0505 %	3.42 %
Ti	53.5700 %	66.05 %

Table S2. Water quality parameters

	pH	IC (mg/L)	TOC (mg/L)	NO_3^- (mg/L)
lake	7.6	19.64	5.1	13.2
river	7.4	20.87	1.04	10.4
tap	6.4	16.71	1.78	12.5

Water quality parameters. The latitude and longitude of the Pearl River water intake point is (113.39, 23.02) and the latitude and longitude of the lake water intake point is (113.39, 23.05).

Table S3. Text for SMT degradation intermediates

number	*m/z*	chemical formula
1	123	$C_6H_9N_3$
2	96	$C_4H_4N_2O$
3	124	$C_6H_8N_2O$
4	214	$C_{12}H_{14}N_4$
5	324	$C_{12}H_{12}N_4O_5S$
6	244	$C_{12}H_{12}N_4O_2$
7	307	$C_{13}H_{15}N_4O_3S$
8	294	$C_{12}H_{14}N_4O_3S$
9	308	$C_{12}H_{12}N_4O_4S$
10	292	$C_{12}H_{12}N_4O_3S$

Fig S1. XPS pattern of Co@MXene and Ti_3AlC_2

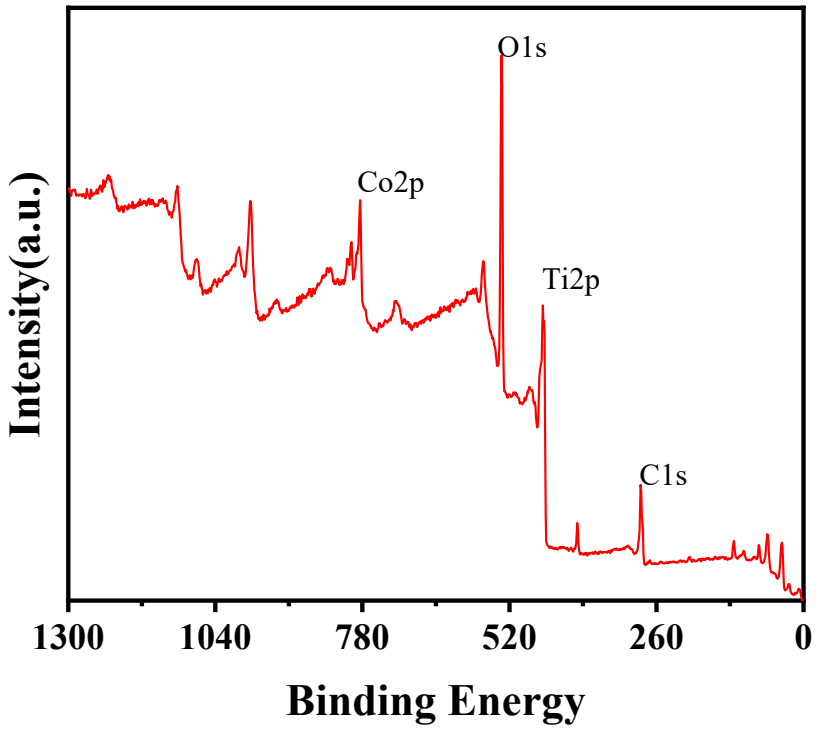

Fig S1. XPS pattern of Co@MXene and Ti_3AlC_2.

Fig S2. SEM image of MAX phase Ti_3AlC_2

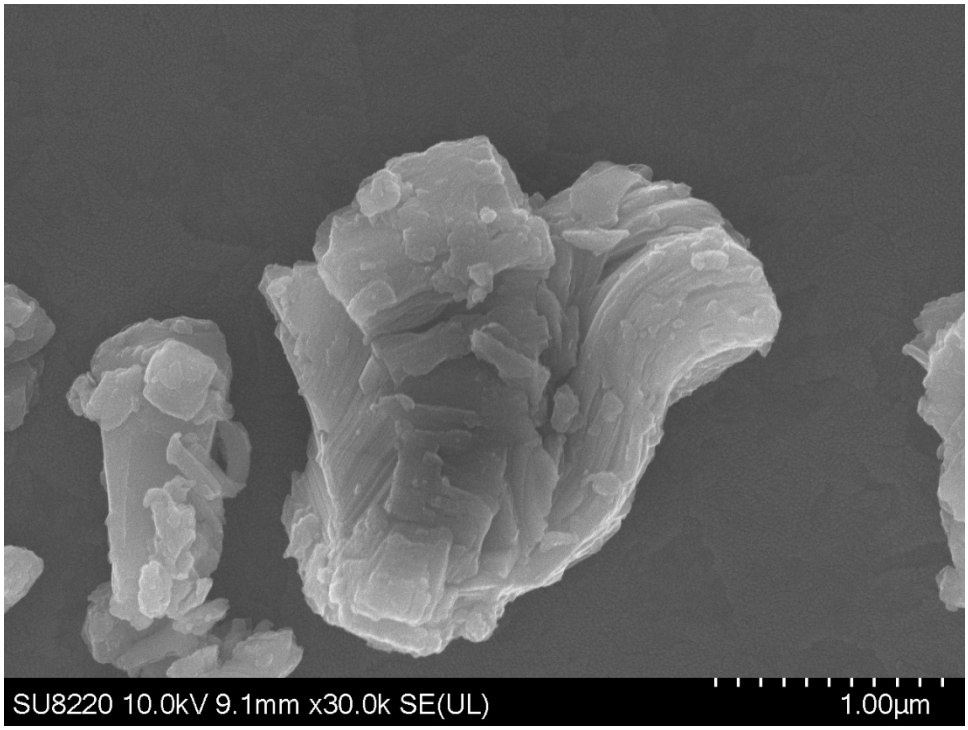

Fig S2. SEM image of MAX phase Ti_3AlC_2.

Fig S3. Degradation of SMT under different conditions

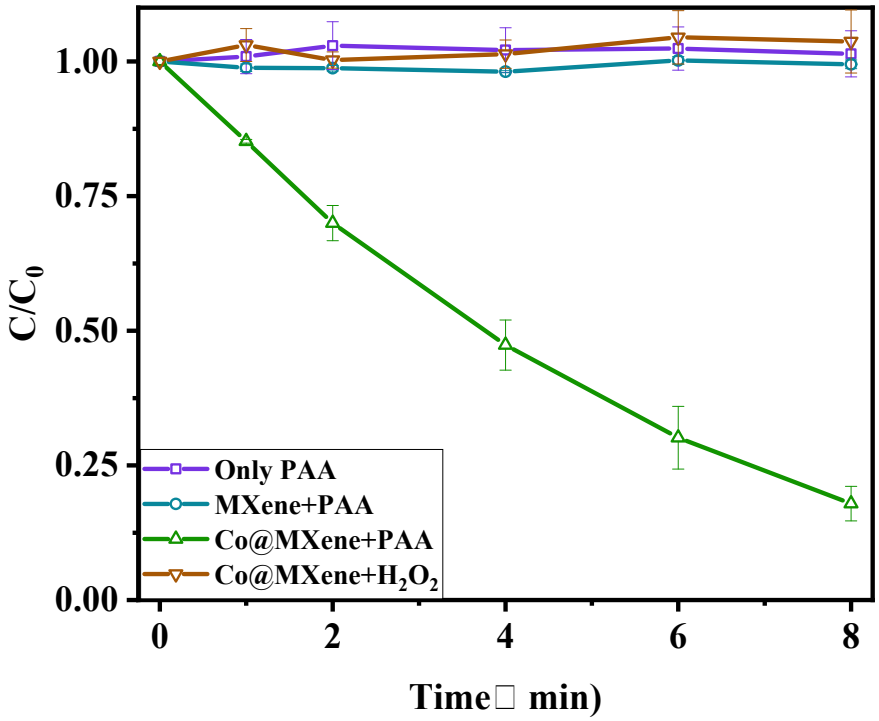

Fig S3. Degradation of SMT under different conditions: $[PAA]_0$ = 0.2 mM, $[catalyst]_0$ = 0.05 g/L, H_2O_2 = 0.8 mM, T = 25 °C.

Fig S4. Detection curve of PAA content during the activation process

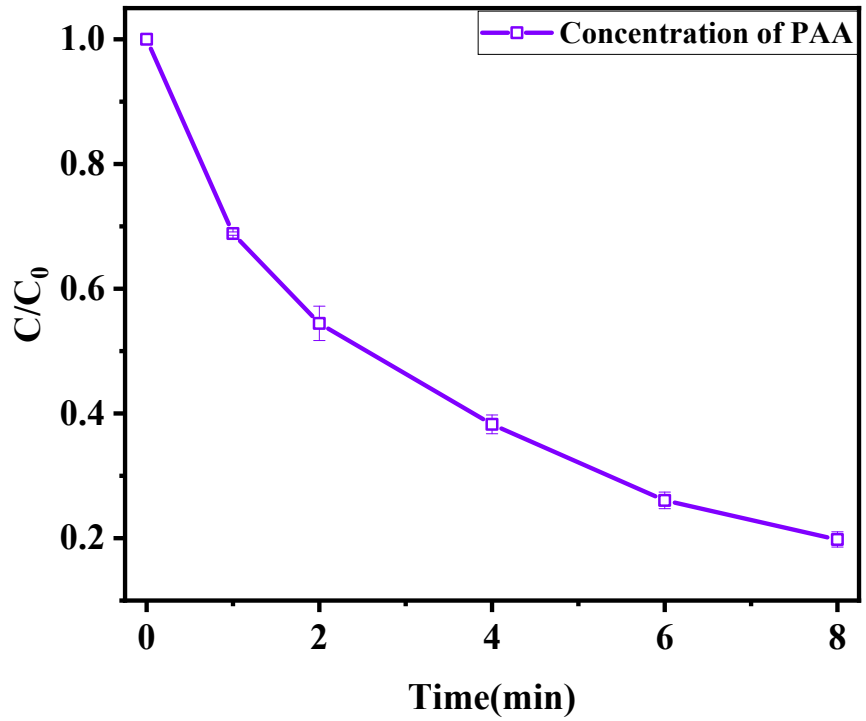

Fig S4. Detection curve of PAA content during the activation process: $[PAA]_0$ = 0.2 mM, $[catalyst]_0$ = 0.05 g/L, t = 25 ℃.

Fig S5. Zeta potential of Co@MXene at different pH conditions

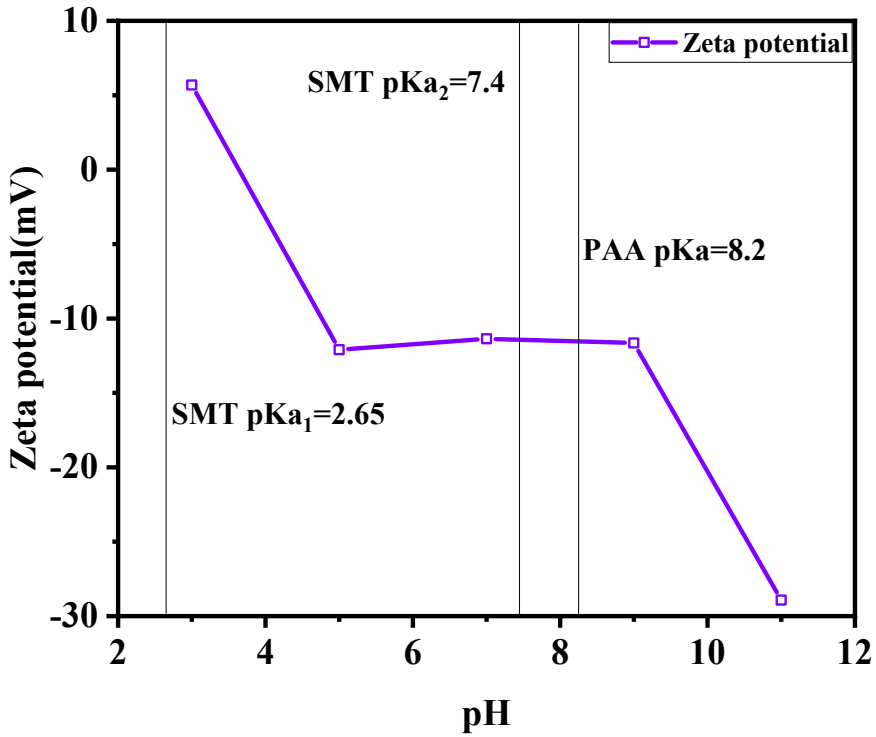

Fig S5. Zeta potential of Co@MXene at different pH conditions.

Fig S6. Organic radical probe secondary mass spectrometry detection plot

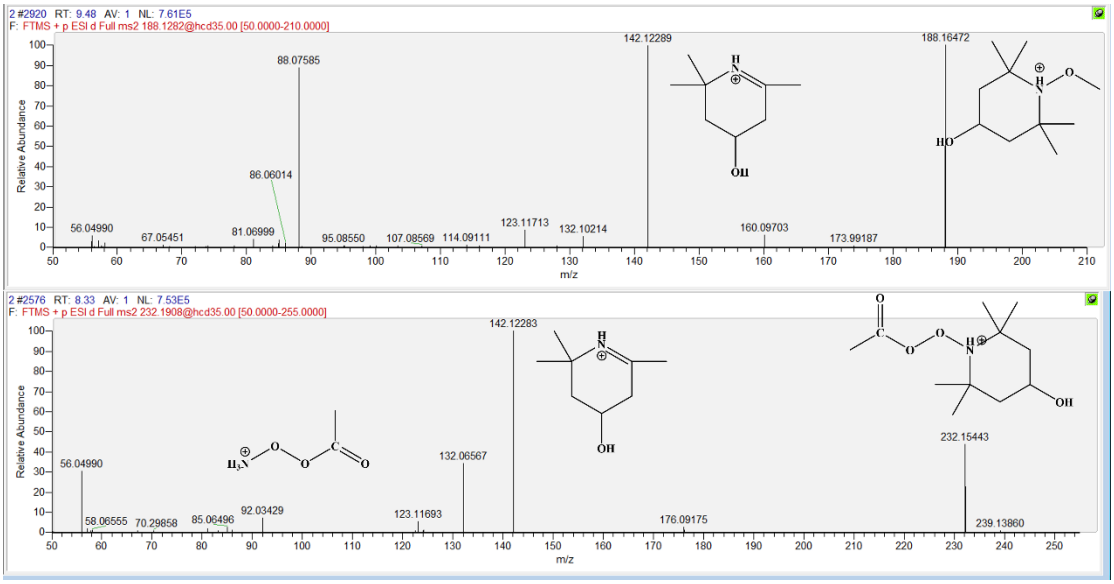

Fig S6. Secondary mass spectra of organic radicals captured by 4-Hydroxy-2,2,6,6-tetramethyl-piperidinooxy; the figure represents the characteristic fragmentation peaks of the captured molecules as well as the structural diagrams.

Fig S7. Degradation profile of SMT under aerobic and anoxic conditions

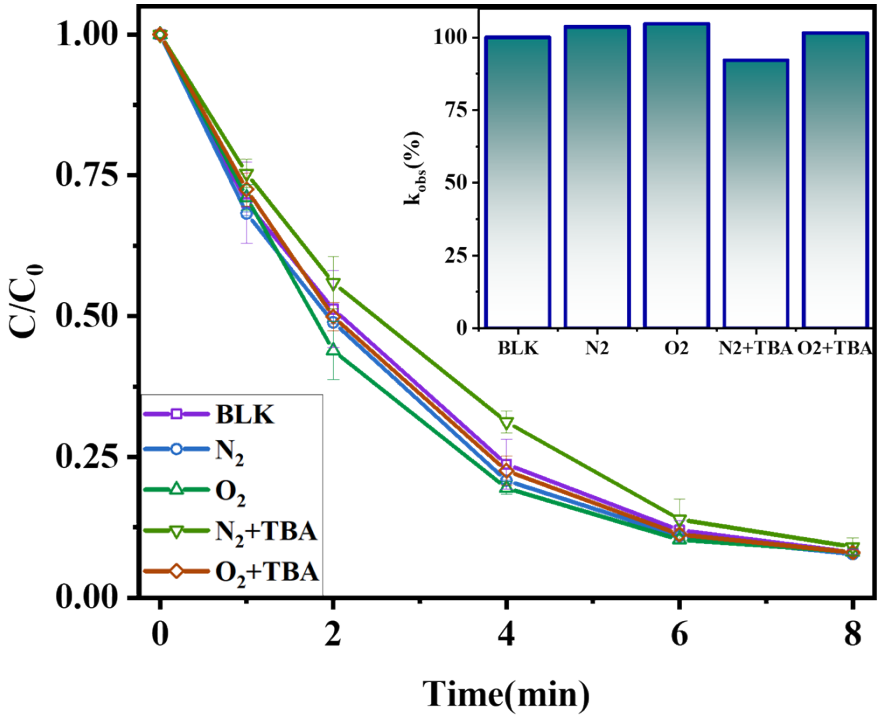

Fig S7. Degradation profile of SMT under aerobic and anoxic conditions; PAA = 0.2 mM, TBA = 100 mM, catalysts = 0.05 g/L, t = 25 ℃.

Fig S8. SMT degradation profile under D_2O and ultrapure water conditions

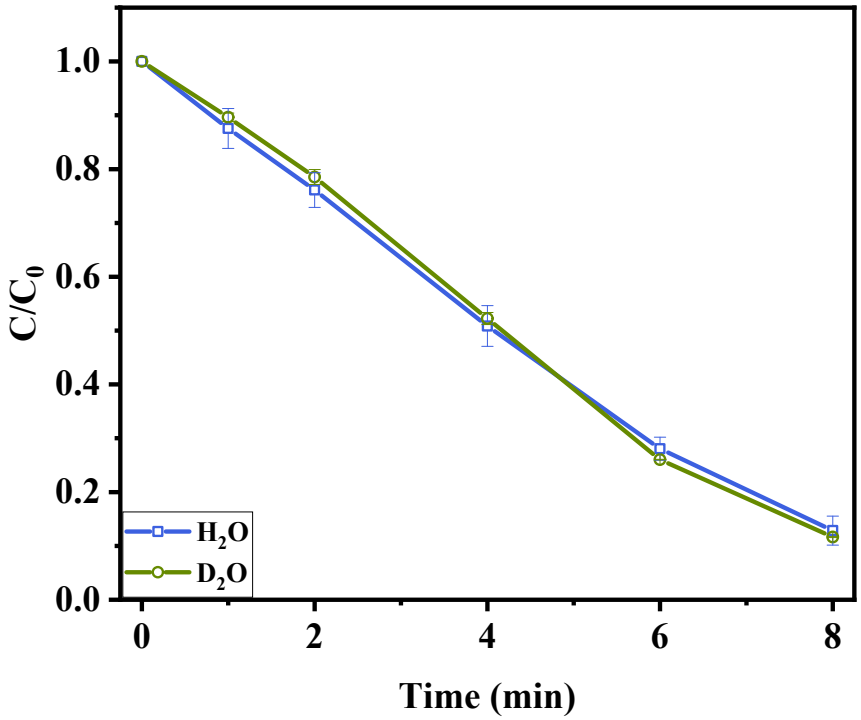

Fig S8. SMT degradation profile under D_2O and ultrapure water conditions: PAA = 0.2 mM, TBA = 100 mM, catalysts = 0.05 g/L, t = 25 ℃.

Fig S9. Time-Open Circuit Voltage Test Curve

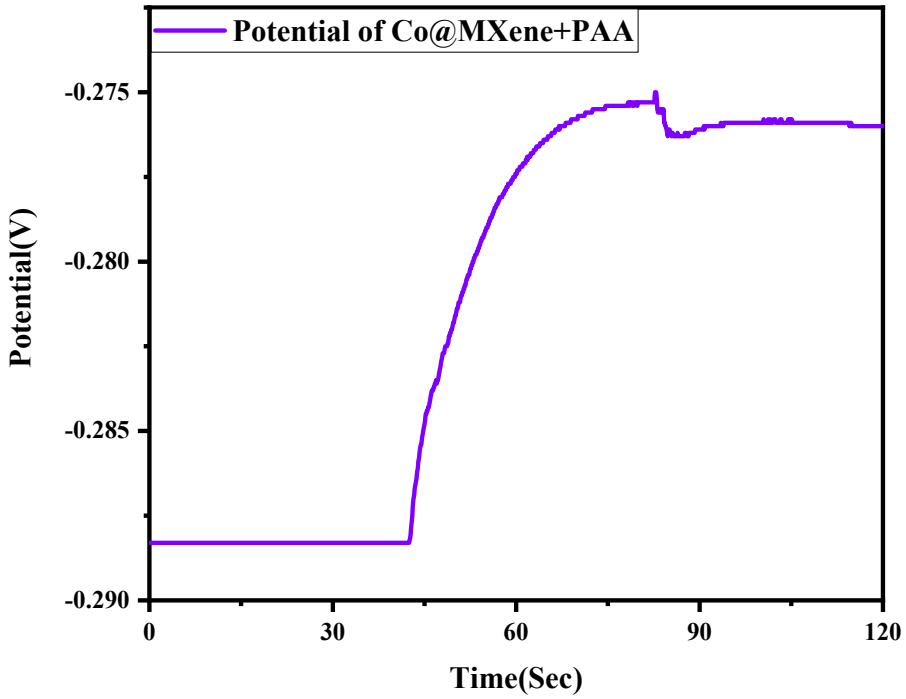

Fig S9. Time-Open Circuit Voltage Test Curve.

Fig S10. DFT computational modelling of high-valent cobalt generation reactions.

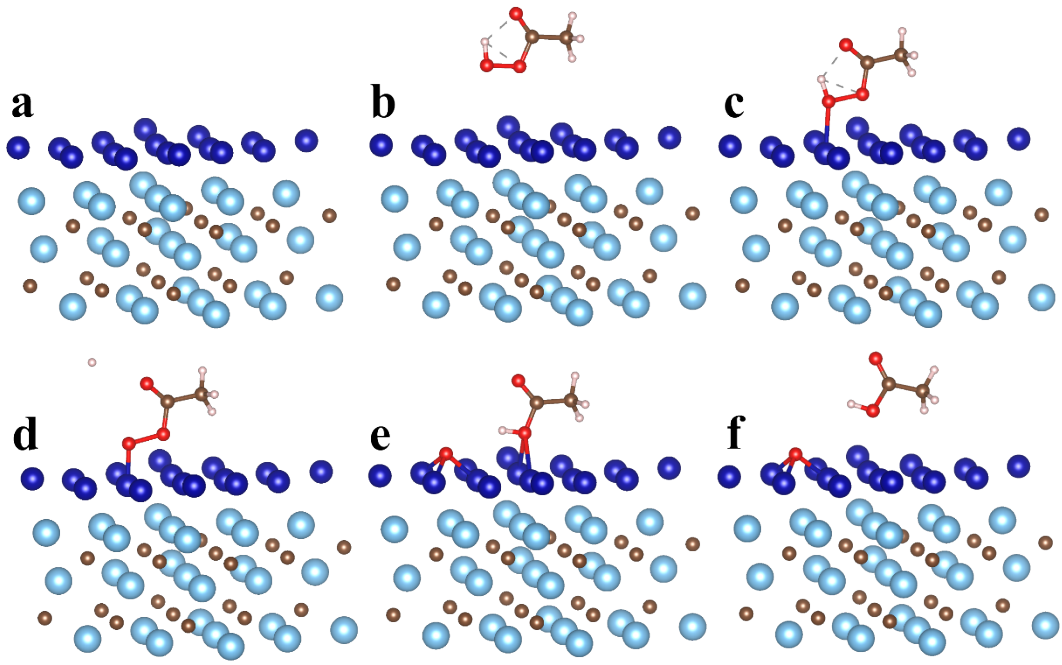

Figure S10. DFT computational modelling of high-valent cobalt generation reactions. Models for (a) ini, (b) INT _1, (c) TS_1, (d) INT _2, (e) TS_2, (f) final.

Fig S11. DFT computational modelling of RO· generation reactions.

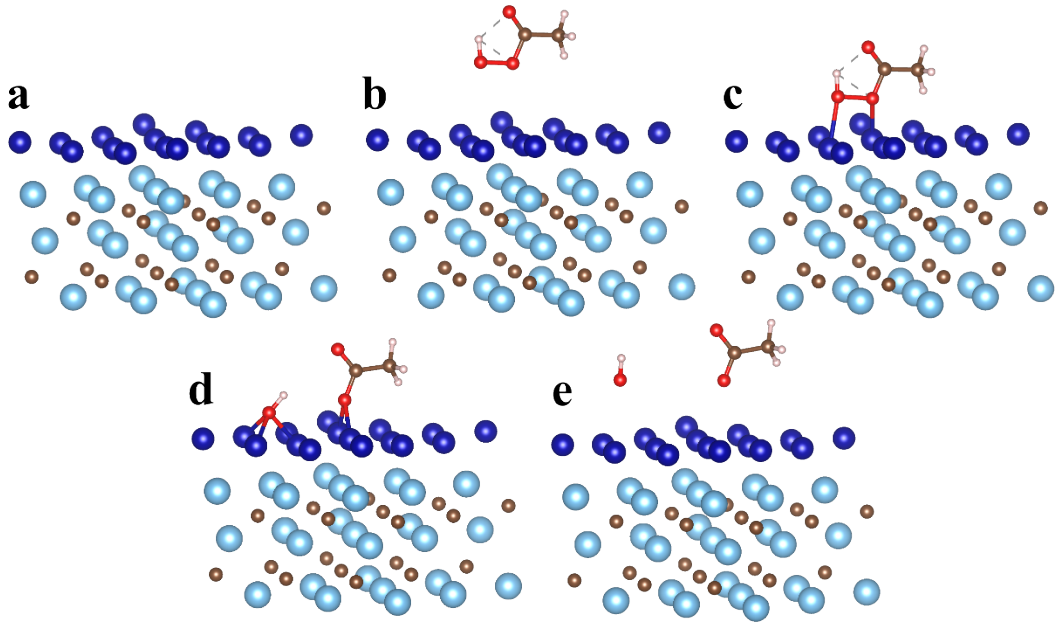

Figure S11. DFT computational modelling of RO· generation reactions. Models for (a) ini, (b) INT _1, (c) TS_1, (d) INT _2, (f) final.

Fig S12. Total Organic Carbon (TOC) test curve

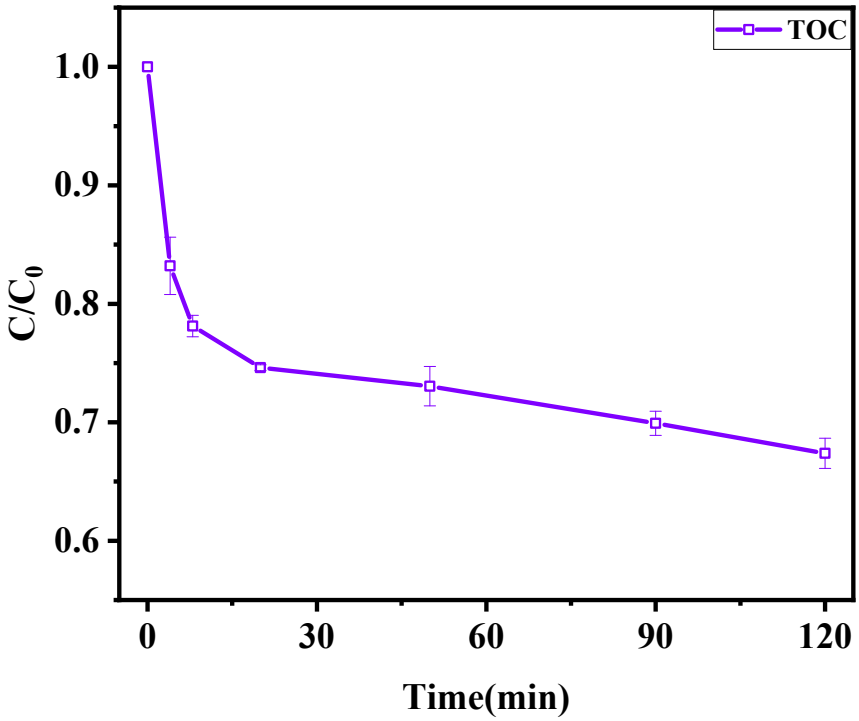

Fig S12. Total Organic Carbon (TOC) test curve.

Fig S13. Ball-and-stick model of sulfadimethoxine-pyrimethamine

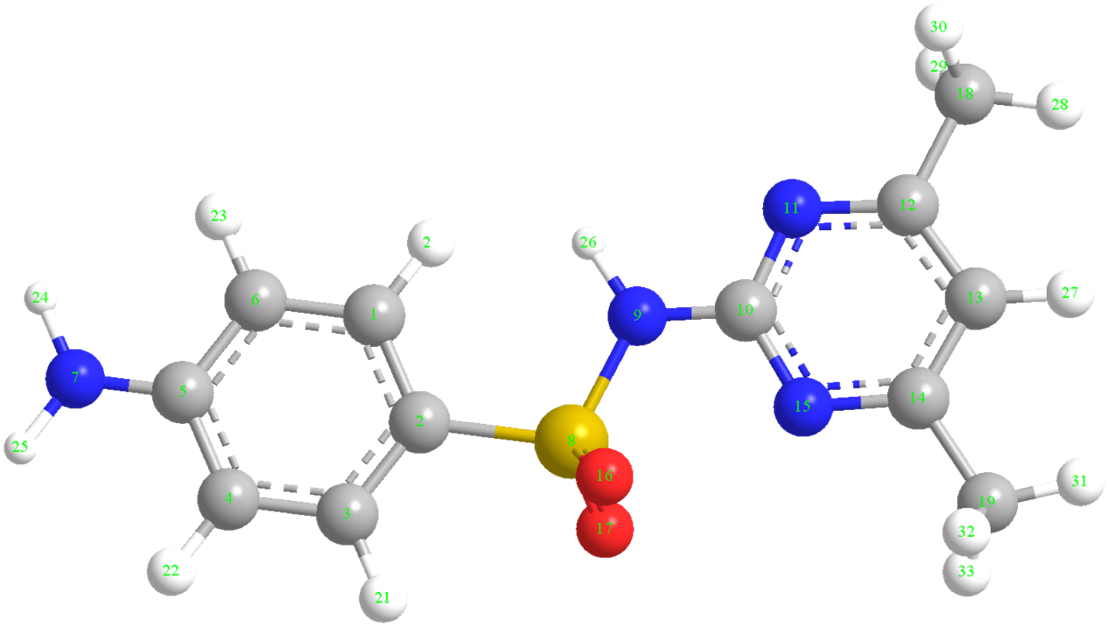

Fig S13. Ball-and-stick model of sulfadimethoxine-pyrimethamine, blue for nitrogen atoms, red for oxygen atoms, yellow for sulphur atoms, grey for carbon atoms.

Fig S14. Partial degradation product DFT calculation model

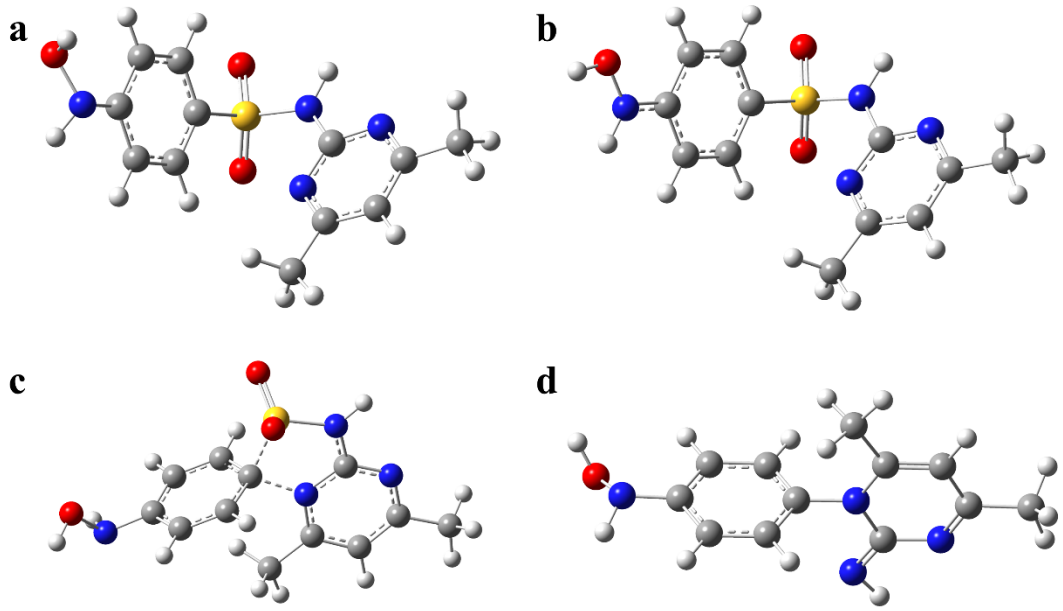

Fig S14. (a) model M1 of product 294; (b) point-bearing positive ion M2 of product 294 after loss of one electron; (c) transition state TS1 of the positive ion rearrangement, and (d) model diagram of the rearrangement of transition state TS1 to produce m3 product 230.

These structures of reactants, products and reaction intermediates were optimized under the framework of density of functional theory (DFT) with m062x functional [10.1007/s00214-007-0310-x] and def2-SVP basis set. The transition state was also searched using the same functional and basis set. All these DFT calculations were performed using Gaussian 16 program suite [Gaussian, Inc., Wallingford CT, 2016].

Fig S15. Excitation-Emission-Matrix Spectra

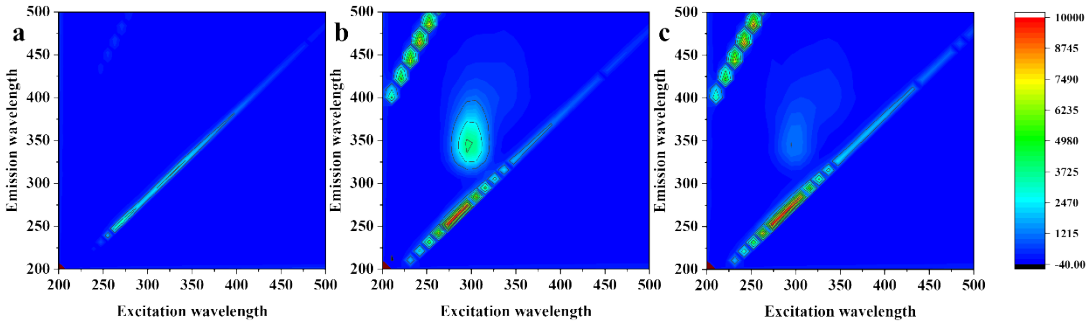

Fig S15. Excitation-emission-matrix spectra of SMT degradation: a) before reaction, b) 2 min, c) after reaction.

Fig S16. Ecotoxicity statistics of intermediate degradates based on ECOSAR simulations

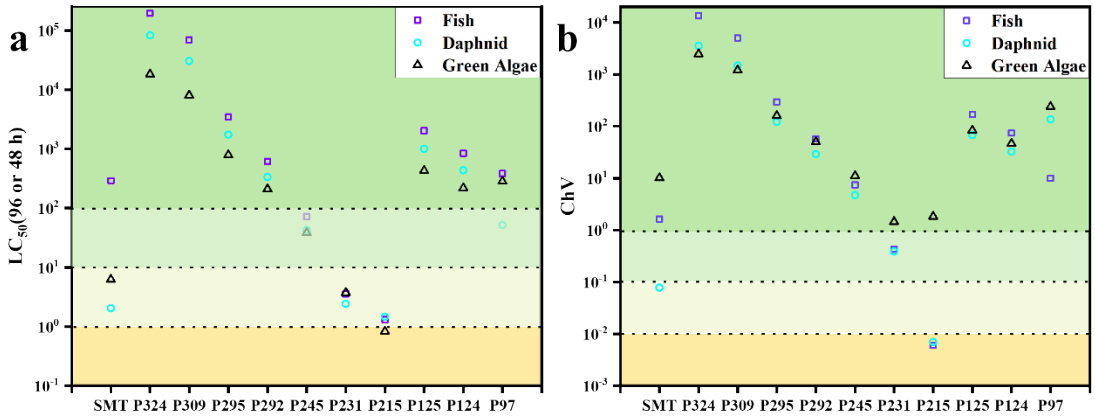

Fig S16. Ecotoxicity statistics for intermediate degradates based on ECOSAR1.1 modelling: a) LC_{50}, b) Chronic toxicity value (ChV).

Fig S17. SMT degradation rate curves at different concentrations of chloride

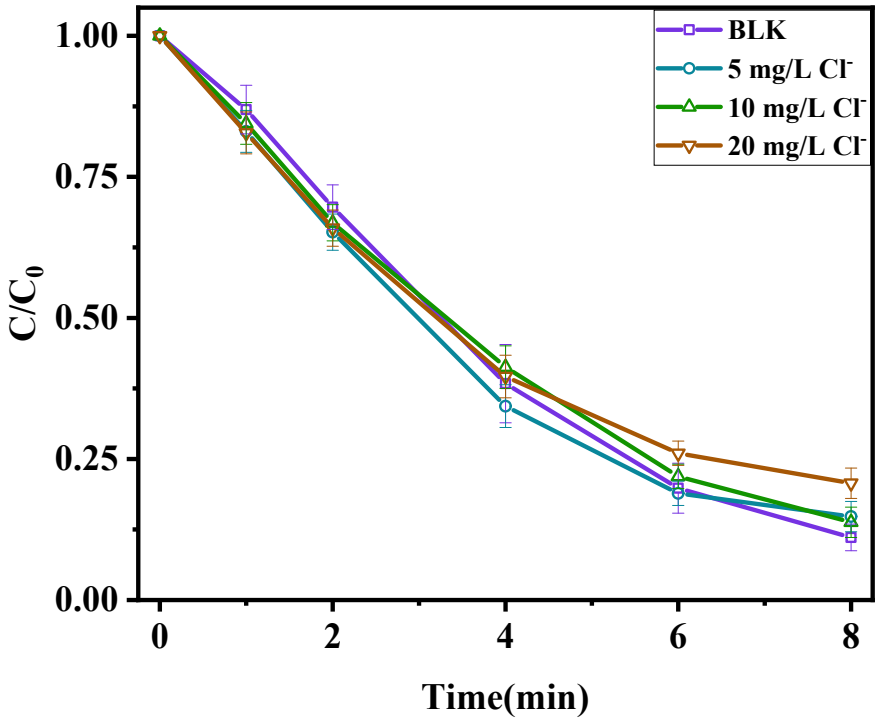

Fig S17. Effect of different concentrations of chloride ions on the degradation of SMT in the Co@MXenes/PAA process: $[PAA]_0$ = 0.2 mM, $[Catalyst]_0$ = 0.05 g/L, t = 25 ℃.

Fig S18. Co@MXene leaching of Co ions for PAA activated degradation of SMT

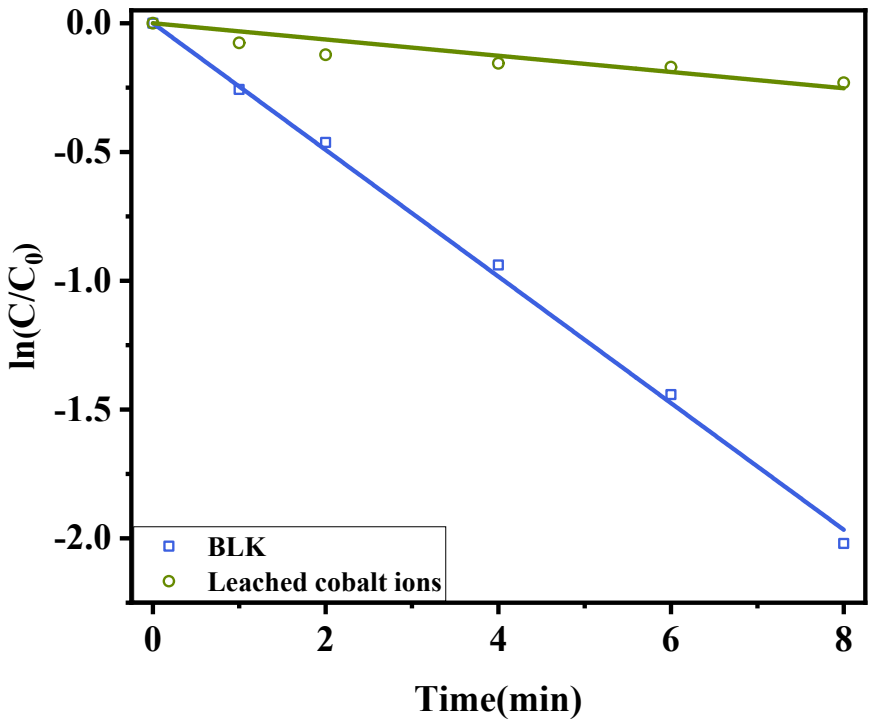

Fig S18. Co@MXene leaching of Co ions for PAA activated degradation of SMT.

Fig S19. Degradation profiles of different types of sulfonamides by Co@MXene/PAA system

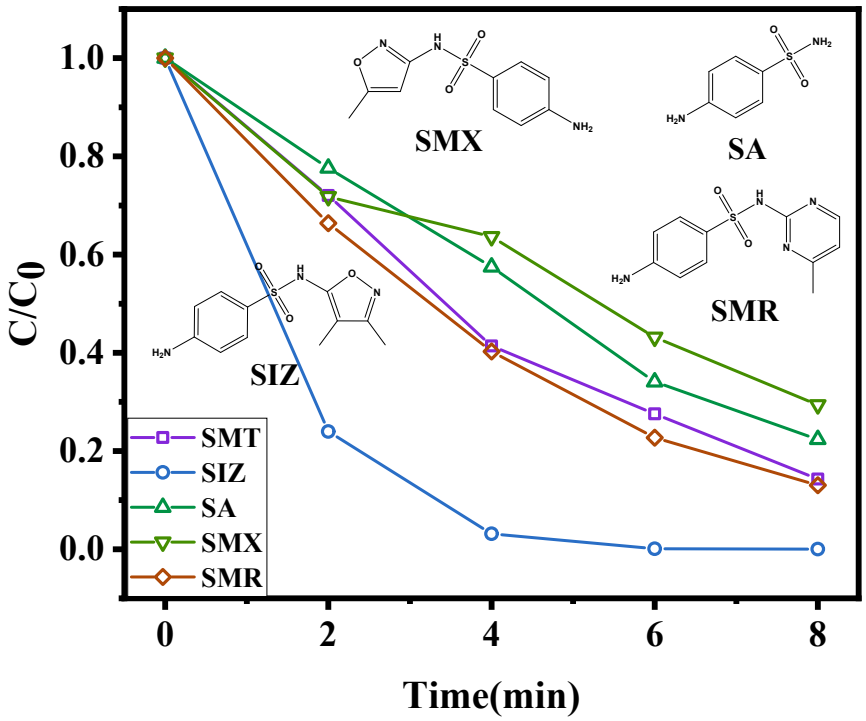

Fig S19. Degradation profiles of different types of sulfonamides by Co@MXene/PAA system. $[contaminant]_0$ =10 mg/L; $[PAA]_0$ = 0.2 mM, $[Catalyst]_0$ = 0.05 g/L, t = 25 ℃.

References

1. T. Zhang and C. H. Huang, Simultaneous quantification of peracetic acid and hydrogen peroxide in different water matrices using HPLC-UV, *Chemosphere*, 2020, **257**, 127229.
2. G. Kresse and J. Furthmüller, Efficiency of ab-initio total energy calculations for metals and semiconductors using a plane-wave basis set, *Computational Materials Science*, 1996, **6**, 15-50.
3. G. Kresse and D. Joubert, From ultrasoft pseudopotentials to the projector augmented-wave method, *Physical Review B*, 1999, **59**, 1758-1775.
4. J. P. Perdew, K. Burke and M. Ernzerhof, Generalized gradient approximation made simple, *PHYSICAL REVIEW LETTERS*, 1996, **77**, 3865-3868.
5. S. Grimme, J. Antony, S. Ehrlich and H. Krieg, A consistent and accurate ab initio parametrization of density functional dispersion correction (DFT-D) for the 94 elements H-Pu, *The Journal of Chemical Physics*, 2010, **132**.
6. D. J. Chadi, SPECIAL POINTS FOR BRILLOUIN-ZONE INTEGRATIONS, *PHYSICAL REVIEW B*, 1977, **16**, 1746-1747.

7. G. Henkelman and H. Jónsson, Improved tangent estimate in the nudged elastic band method for finding minimum energy paths and saddle points, *The Journal of Chemical Physics*, 2000, **113**, 9978-9985.